

Composition- and pressure-induced ferroelectric to antiferroelectric phase transitions in Sm-doped BiFeO₃ system

Fei Xue, Linyun Liang, Yijia Gu, Ichiro Takeuchi, Sergei V. Kalinin, and Long-Qing Chen

Citation: [Applied Physics Letters](#) **106**, 012903 (2015); doi: 10.1063/1.4905444

View online: <http://dx.doi.org/10.1063/1.4905444>

View Table of Contents: <http://scitation.aip.org/content/aip/journal/apl/106/1?ver=pdfcov>

Published by the [AIP Publishing](#)

Articles you may be interested in

[Combined effects of Bi deficiency and Mn substitution on the structural transformation and functionality of BiFeO₃ films](#)

J. Appl. Phys. **116**, 174102 (2014); 10.1063/1.4901323

[Pressure effect on structural and vibrational properties of Sm-substituted BiFeO₃](#)

J. Appl. Phys. **114**, 154110 (2013); 10.1063/1.4826069

[Multiferroic and structural properties of BiFeO₃ close to the strain induced phase transition on different substrates](#)

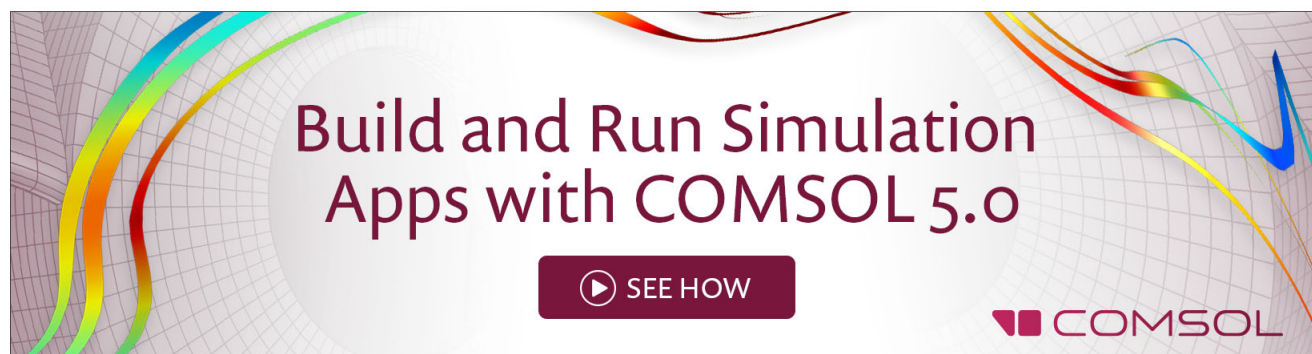
J. Appl. Phys. **113**, 17D907 (2013); 10.1063/1.4795216

[Improved multiferroic properties in Sm-doped BiFeO₃ thin films deposited using chemical solution deposition method](#)

J. Appl. Phys. **111**, 102801 (2012); 10.1063/1.4714650

[Terahertz and infrared studies of antiferroelectric phase transition in multiferroic Bi_{0.85}Nd_{0.15}FeO₃](#)

J. Appl. Phys. **110**, 074112 (2011); 10.1063/1.3650241

A promotional banner for COMSOL 5.0. The background is a light gray grid with several colorful, flowing lines in shades of blue, green, yellow, and red. The text 'Build and Run Simulation Apps with COMSOL 5.0' is centered in a dark red, serif font. Below the text is a dark red button with a white play icon and the text 'SEE HOW'. In the bottom right corner, the COMSOL logo is displayed, consisting of three red squares followed by the word 'COMSOL' in a dark red, sans-serif font.

Composition- and pressure-induced ferroelectric to antiferroelectric phase transitions in Sm-doped BiFeO₃ system

Fei Xue,¹ Linyun Liang,¹ Yijia Gu,¹ Ichiro Takeuchi,² Sergei V. Kalinin,³ and Long-Qing Chen¹

¹Department of Materials Science and Engineering, Pennsylvania State University, University Park, Pennsylvania 16802, USA

²Department of Materials Science and Engineering, University of Maryland, College Park, Maryland 20742, USA

³The Center for Nanophase Materials Sciences, Oak Ridge National Laboratory, Oak Ridge, Tennessee 37831, USA

(Received 26 October 2014; accepted 20 December 2014; published online 5 January 2015)

A three-dimensional phenomenological model is proposed to describe both ferroelectricity and antiferroelectricity based on the Ginzburg-Landau-Devonshire theory. Its application to the multi-ferroic Sm-doped BiFeO₃ system describes the temperature-, pressure-, and composition-induced ferroelectric to antiferroelectric phase transitions. The constructed temperature-composition and temperature-pressure phase diagrams show that compressive hydrostatic pressure and Sm doping have similar effects on the ferroelectric and antiferroelectric phase transitions. It is also indicated from the temperature-pressure phase diagram that the experimentally observed phase of BiFeO₃ under the hydrostatic pressure from 3 GPa to 10 GPa is a PbZrO₃-like antiferroelectric phase.

© 2015 AIP Publishing LLC. [<http://dx.doi.org/10.1063/1.4905444>]

An antiferroelectric (AFE) phase is defined as an antipolar crystal with antiparallel cation displacements of neighboring unit cells in contrast to a polar ferroelectric (FE) phase, in which the cation displacements in neighboring unit cells are all parallel to each other.¹ When subjected to a sufficiently high external electric field, AFE crystals may undergo an AFE to FE phase transition, and the process is characterized by the double-hysteresis loops. Accompanying the phase transition, physical properties, such as linear dimensions and optical properties, may change significantly, which provide the physical foundation for engineering applications of AFE materials in digital displacement transducers² and energy storage capacitors.³

The very first theoretical model to describe an AFE phase was a simple two-sublattice model by Kittel,⁴ proposed before the experimental confirmation of the existence of AFEs.⁵ Cross and Okada developed a phenomenological model by writing the Gibbs free energy as a function of two dependent FE and AFE order parameters.⁶ Haun *et al.* employed a three-dimensional FE-AFE model to study the antiferroelectricity in PbZrO₃ by assuming an orthorhombic symmetry.⁷ Balashova and Tagantsev presented a one-dimensional (1D) phenomenological model with competing structural and FE instabilities and studied dielectric responses under applied electric fields.⁸ Recently, the origin of antiferroelectricity is discussed based on the lattice dynamics in PbZrO₃.⁹ However, most of the current phenomenological theories focus on the AFE to FE phase transition induced by applied electric fields^{6,8} rather than by hydrostatic pressure although experimental observations showed that the inter-AFE phase transition is very sensitive to the applied pressure.¹⁰⁻¹³ Furthermore, no existing models can be directly applied to determining temperature-composition as well as temperature-pressure phase diagrams involving both FE and AFE phases of a specific system.

In this letter, we modify the phenomenological theory of Cross and Okada by defining independent FE and AFE order parameters. The Sm-doped BiFeO₃ (BFO) system is chosen as a particular example. Pure BFO is an ABO₃ perovskite-type oxide with space group *R3c* at room temperature, while above 825 °C, it shows an orthorhombic paraelectric (PE) crystal structure with space group *Pnma*.^{14,15} At room temperature, Bi_{1-x}Sm_xFeO₃ is determined to be the PbZrO₃-type AFE structure for *x* ranging from 0.1 to 0.16,¹⁶⁻¹⁸ and the *Pnma* phase for *x* larger than 0.16.¹⁸⁻²⁰ Based on these experimental data, a temperature-composition phase diagram is constructed. Furthermore, we incorporate the interaction between the FE (AFE) order parameter and hydrostatic pressure. The derived relationship between transition temperatures and pressure corresponds to the well-known Clapeyron Equation. The calculated temperature-pressure phase diagram for pure BFO indicates that the intermediate phase under the pressure between 3.5 and 10 GPa is the PbZrO₃-like AFE phase.

To describe the FE and AFE phases, the Sm-doped BFO crystal is divided into two sublattices, *a* and *b*, associated with polarizations \vec{P}_a and \vec{P}_b , respectively. If \vec{P}_a and \vec{P}_b are parallel to each other, the system exhibits the FE phase as sketched in Fig. 1(a). On the other hand, it is the AFE phase if \vec{P}_a and \vec{P}_b are antiparallel, as illustrated in Fig. 1(b). When \vec{P}_a and \vec{P}_b are both zero, it is the PE phase.

The FE and AFE order parameters \vec{p} and \vec{q} are defined as follows:

$$\vec{p} = \frac{1}{2}(\vec{P}_a + \vec{P}_b), \quad \vec{q} = \frac{1}{2}(\vec{P}_a' - \vec{P}_b'). \quad (1)$$

In Eq. (1), we use \vec{P}_a' and \vec{P}_b' , instead of \vec{P}_a and \vec{P}_b , for the definition of the AFE order parameter, to emphasize that the polarizations associated with the sublattices of the

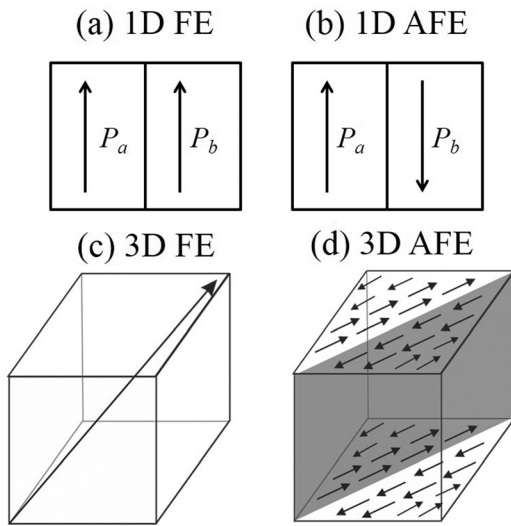


FIG. 1. Schematic plot of the FE and AFE phases.

AFE phase are sometimes different from those of the FE phase. It indicates that the AFE to FE phase transition does not only involve the flip of the polarization in one of the two sublattices but also the changes in the magnitude and direction of the polarizations.²¹ As shown in Figs. 1(c) and 1(d), in the Sm-doped BFO system, the spontaneous polarization is along the [111] direction for the FE phase, while it is along [110] for the AFE phase.¹⁷ It should be noted that here we use the conventionally definition of AFE, i.e., an AFE phase is a PbZrO₃-like phase with quadrupled unit cells, as shown in Fig. 1(d).

The stable phases of interest in the Sm-doped BFO system are listed in Table I. Note that in the FE, AFE, and PE phases, there exist the oxygen octahedral tilt instabilities, besides the polar and antipolar instabilities.¹⁴ Therefore, the thermodynamic free energy that we employ can be considered as an effective energy function by implicitly including the contributions from oxygen octahedral tilt instabilities. In this scheme, however, the *Pnma* and high symmetry cubic phases are indistinguishable. In this letter, the *Pnma* to cubic phase transition is neglected, and the PE phase is assumed to have the cubic symmetry while maintaining the same free energy and volume with the *Pnma* phase, i.e., the PE phase is an imaginary phase that does not exist in reality.

Taking the unpolarized and unstressed PE phase at the same temperature and composition as the reference state, the total free energy density of the Sm-doped BFO system under the stress-free boundary conditions can be expressed as

$$f_{total}|_{\sigma=0} = a_{ij}p_i p_j + a_{ijkl}p_i p_j p_k p_l + a_{ijklmn}p_i p_j p_k p_l p_m p_n + b_{ij}q_i q_j + b_{ijkl}q_i q_j q_k q_l + b_{ijklmn}q_i q_j q_k q_l q_m q_n + t_{ijkl}p_i p_j q_k q_l, \quad (2)$$

TABLE I. Order parameters of different phases.

| Phases | Order parameters |
|-----------|--------------------------------------|
| PE phase | $p_i = 0, q_i = 0$ |
| FE phase | $p_1 = p_2 = p_3 \neq 0, q_i = 0$ |
| AFE phase | $p_i = 0, q_1 = q_2 \neq 0, q_3 = 0$ |

where p_i and q_i are the i th components of the FE and AFE order parameters in the pseudocubic coordinate system; a_{ij} , a_{ijkl} , and a_{ijklmn} are the FE dielectric stiffnesses; b_{ij} , b_{ijkl} , and b_{ijklmn} are the AFE dielectric stiffnesses; and t_{ijkl} are coupling coefficients between the FE and AFE order parameters. $\sigma = 0$ refers to the reference external pressure, i.e., ambient pressure. The FE and AFE Landau free energy polynomial functions are expanded to sixth order to include the characteristics of the first-order phase transition,^{14,19} and to stabilize the orthorhombic AFE phase.²² Among all the coefficients, only a_{11} and b_{11} are assumed to be dependent on composition and temperature, i.e., $a_{11} = a_0[T - T_c(x)]$ and $b_{11} = b_0[T - T_q(x)]$, where a_0 and b_0 are constants; x denotes the Sm composition; and $T_c(x)$ and $T_q(x)$ are the FE and AFE Curie temperatures at composition x , respectively. It is assumed that both $T_c(x)$ and $T_q(x)$ have linear relationships with x as $T_c(x) = T_{c0}(1 - c_p x)$ and $T_q(x) = T_{q0}(1 - c_q x)$,²³ where c_p and c_q are constants; and T_{c0} and T_{q0} are the FE and AFE Curie temperatures of pure BFO, respectively. The Landau free energy expansion coefficients of the FE and AFE phases are obtained by fitting the free energy to the corresponding experimental results and phase diagram data.^{19,20,24,25} For simplicity, the coupling term is only expanded to fourth order. In order to suppress the following phase, $p \neq 0, q \neq 0$,^{8,26} t_{ij} is assumed to be sufficiently positive. All the coefficients needed for the calculations are listed in Table II.

According to the thermodynamic stability conditions, $\frac{\partial F_{total}}{\partial p_i} = 0, \frac{\partial F_{total}}{\partial q_i} = 0$, we obtain the equilibrium values of p_i and q_i for all the stable and metastable phases. Substituting these equilibrium values back into Eq. (2), the total energies for different phases can then be determined.

The free energies of the FE and AFE phases of pure BFO with different symmetries as a function of temperature are plotted in Figs. 2(a) and 2(b), respectively. It can be seen that the rhombohedral symmetry is stable for the FE phase while the orthorhombic symmetry is stable for the AFE phase. The comparison of the free energies for the rhombohedral FE and orthorhombic AFE phases for different Sm compositions at room temperature is shown in Fig. 2(c), which illustrates that the FE, AFE, and PE phases are stable when the Sm composition is smaller than 0.1, between 0.1 and 0.16, and larger than 0.16, respectively. The polarization component p_1 of pure BFO as a function of temperature is plotted in Fig. 2(d), indicating a first-order phase transition at 825 °C. The magnitude of p_1 at room temperature is about 0.6 C/m², and thus total polarization is $p_S = \sqrt{3}p_1 \approx 1\text{C/m}^2$, which is consistent with the experimentally measured value.²⁷

TABLE II. Coefficients of Sm_xBi_{1-x}FeO₃ used in the calculation (SI units).

| a_0 | 1.093×10^5 | b_0 | 9.492×10^4 |
|--------------------|-----------------------------|--------------------------------|-----------------------------|
| $T_c(x)$ | $815 - 5.314 \times 10^3 x$ | $T_q(x)$ | $815 - 5.031 \times 10^3 x$ |
| a_{1111} | 3.500×10^7 | b_{1111} | 2.000×10^7 |
| a_{1122} | -7.222×10^7 | b_{1122} | -9.692×10^7 |
| a_{111111} | 1.200×10^8 | b_{111111} | 2.000×10^7 |
| a_{111122} | 1.619×10^7 | b_{111122} | 1.222×10^8 |
| a_{112233} | 4.934×10^8 | b_{112233} | 1.000×10^{11} |
| $Q_{11} + 2Q_{12}$ | 0.011 | $\Lambda_{11} + 2\Lambda_{12}$ | 7.641×10^{-3} |

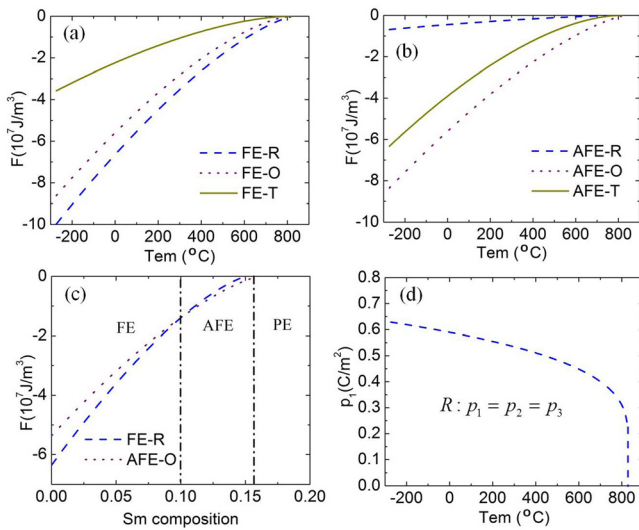


FIG. 2. The free energies of (a) the FE phases and (b) the AFE phases with different symmetries of pure BFO as a function of temperature: tetragonal (T) symmetry with only one nonzero component, orthorhombic (O) with two nonzero components, and rhombohedral (R) with three nonzero components. (c) The free energies of the rhombohedral FE and orthorhombic AFE phases as a function of the Sm composition at room temperature 25 °C. (d) The polarization component (p_1) of pure BFO as a function of temperature in the rhombohedral FE phase.

Figure 3(a) shows the calculated temperature-composition phase diagram of the Sm-doped BFO system at ambient pressure, which is in a good agreement with experiment observation.²⁰ The PE-AFE and AFE-PE phase boundaries are straight lines, which is due to the assumption that only a_{11} and b_{11} are linearly dependent on composition, as shown in Table II.

The total free energy density including the elasticity contribution can be written as

$$f_{total} = f_{total}|_{\sigma=0} + \frac{1}{2} S_{ijkl} \sigma_{ij} \sigma_{kl} - Q_{ijkl} p_i p_j \sigma_{kl} - \Lambda_{ijkl} q_i q_j \sigma_{kl}, \quad (3)$$

where S_{ijkl} is the compliance tensor; σ_{ij} denotes the stress tensor; and Q_{ijkl} and Λ_{ijkl} are the FE and AFE electrostrictive coefficients, respectively. The electrostrictive coefficients are obtained from the experimentally measured lattice parameters^{28–30} by assuming that the lattice parameters are linearly dependent on pressure.

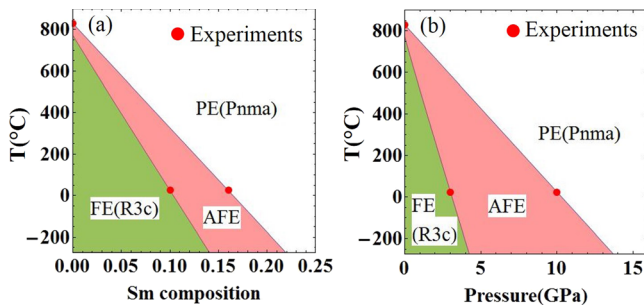


FIG. 3. (a) Temperature-composition phase diagram of Sm-doped BFO at ambient pressure; (b) temperature-pressure phase diagram of pure BFO. The FE, PE, and AFE phases are denoted by green, white, and pink colors, respectively. The red dots are taken from experimental data.^{14,20}

By rearranging the free energy of the FE phase under hydrostatic pressure ($\sigma_1 = \sigma_2 = \sigma_3 = \sigma$, $\sigma_4 = \sigma_5 = \sigma_6 = 0$) and following the Voigt notation, the relationship between the FE Curie temperature and the hydrostatic pressure can be written as

$$T_c(x, \sigma) = T_c(x) + \frac{1}{a_0} (Q_{11} + 2Q_{12}) \sigma. \quad (4)$$

Equation (4) shows that the FE Curie temperature is linearly dependent on pressure and the linear coefficient is proportional to $Q_{11} + 2Q_{12}$. According to the infinitesimal strain theory,³¹ the relative variation of the volume or dilatation can be expressed as a summation of the normal strains, i.e., $\Delta = \varepsilon_{11} + \varepsilon_{22} + \varepsilon_{33}$. The phase transition strain is given in terms of p_i and q_i ,³² $\varepsilon_{ij} = Q_{ijkl} p_k p_l + \Lambda_{ijkl} q_k q_l$. For the FE phase ($p_1 = p_2 = p_3 = p$, $q_1 = q_2 = q_3 = 0$), the dilatation relative to the PE phase during the phase transition is

$$\Delta_p = \varepsilon_{11} + \varepsilon_{22} + \varepsilon_{33} = 3(Q_{11} + 2Q_{12}) p^2. \quad (5)$$

The entropy change ΔS per volume is given by

$$\Delta S = \frac{\partial f_{FE}}{\partial T} = 3a_0 p^2. \quad (6)$$

In Eqs. (5) and (6), p is the magnitude of polarization just below the transition temperature. Since all the coefficients except a_{11} are independent of pressure and temperature and only the lowest-order coupling terms between polarization and stress are considered, p is a constant for the above first-order transition (this is valid only for a small pressure range, since pressure may change the order of the transition³³). Therefore, Δ_p and ΔS are independent of temperature and pressure based on the model. From Eqs. (4)–(6), we have

$$\frac{\partial T_c(x, \sigma)}{\partial \sigma} = \frac{Q_{11} + 2Q_{12}}{a_0} = \frac{\Delta_p}{3a_0 p^2} = \frac{\Delta_p}{\Delta S}. \quad (7)$$

For a first-order transition, the FE phase transition temperature is related to the Curie temperature by

$$T_c^t(x, \sigma) = T_c(x, \sigma) + \frac{3(a_{1111} + a_{1122})^2}{4a_0(3a_{111111} + 6a_{111122} + a_{112233})}. \quad (8)$$

Only $T_c(x, \sigma)$ is dependent on the pressure, and thus, we obtain

$$\frac{\partial T_c^t(x, \sigma)}{\partial \sigma} = \frac{\Delta_p}{\Delta S} = \frac{\Delta V_p / V}{\Delta S_p / V} = \frac{\Delta V_p}{\Delta S_p}, \quad (9)$$

where V , ΔV_p , and ΔS_p are the system volume, volume change, and entropy change, respectively. Similarly, for the AFE phase transition, we have

$$\frac{\partial T_q^t(x, \sigma)}{\partial \sigma} = \frac{\Delta V_q}{\Delta S_q}. \quad (10)$$

Equations (9) and (10) are essentially the well-known Clapeyron Equations. The Clapeyron Equation indicates that

for a first-order phase transition, the derivative of transition temperature with respect to pressure is determined by the volume and enthalpy changes between the two phases.

By minimizing the total free energy in Eq. (3), we constructed a temperature-pressure phase diagram for pure BFO, as shown in Fig. 3(b). Three phases (the FE, AFE, and PE phases) are identified similarly to the temperature-composition phase diagram in Fig. 3(a). The AFE-PE phase boundary is a straight line as illustrated by Eq. (10). The AFE-FE phase boundary is also a straight line, which is similar to the AFE-FE transition in tin-modified lead zirconate titanate (PZT) ceramics.¹² The linear dependence of transition temperatures on pressure comes from the fact that only the lowest-order coupling terms between the order parameters and stress are maintained, and from the assumption that all the stiffness coefficients are independent of pressure.

The “chemical pressure” (replacing the cations with larger or smaller cations) may produce a similar effect as pressure on promoting the FE and AFE phase transitions. For example, in the PZT system, either adding zirconium or applying pressure can induce the FE *R3c* to AFE *Pbam* phase transition for the low titanium content PZT,^{11,34} and the FE *P4mm* to PE *Pm3m* phase transition for the high titanium content PZT,^{34,35} respectively. Here, we propose a phenomenological theory to describe the similarity between the chemical pressure and hydrostatic pressure, as shown in Fig. 3.

Although pure BFO is experimentally determined to exhibit the *Pnma* symmetry under pressure between 10 GPa and 20 GPa,^{24,29,36} there are discrepancies among different studies on the stable phases with pressure ranging from 3 GPa to 10 GPa. Possible intermediate symmetries include *C2/m*,²⁹ *O1* and *O2*,³⁷ *Pbam*,³⁰ and *O1*, *O2*, and *O3*.²⁴ Based on our calculations, the PbZrO₃-like *Pbam* phase better reflects the similarities between the chemical pressure and hydrostatic pressure, which is obtained from the neutron diffraction results.³⁰ It is believed that the neutron diffraction result is more accurate than the X-ray, since the X-ray is less sensitive to the oxygen ions than the Bi and Fe ions. We speculate that the different phases observed by other groups are produced by the twin structures of *R3c* and *Pbam* phases. Furthermore, the relationship between the FE and AFE phases in the Sm-doped BFO system resembles that on the low titanium content side of the PZT system.^{18,20} In both systems, the FE to AFE phase transition occurs with a decrease in the tolerance factor. The tolerance factor (*t*) is an indicator for the stabilities of the structural distortions in perovskites ABO₃, and is given by $t = (R_A + R_O) / \sqrt{2} (R_B + R_O)$, where *R_A*, *R_B*, and *R_O* are the ionic radii of the A, B, and O elements, respectively.²⁰ It should be noted that for the Sm-doped BFO, it is A-site doping, and the tolerance factor decreases because of the smaller atom substitutions. On the other hand, in the PZT system, it is B-site doping, and the decrease in the tolerance factor is due to adding bigger zirconium atoms. The similarities between the Sm-doped BFO and PZT systems serve as indirect evidences that the BFO phase under the pressure between 3 GPa and 10 GPa is the PbZrO₃-like AFE phase.

The temperature-pressure phase diagram in Fig. 3(b) shows that hydrostatic pressure can induce the FE to AFE to PE phase transitions. This can be explained by the volume

differences, i.e., $V_{FE} > V_{AFE} > V_{PE}$. In other systems, usually $V_{FE} > V_{AFE}$ and $V_{FE} > V_{PE}$ are observed, and pressure can induce the FE to PE and FE to AFE phase transitions.^{10–12} However, if the pseudocubic unit cell of the AFE phase is smaller than that of the PE phase, applying the pressure will favor the AFE phase rather than the PE phase. For example, in the modified PZT system, it is shown that pressure can increase the PE to AFE transition temperature because of $V_{AFE} < V_{PE}$.^{10,13,38}

In summary, we proposed a modified phenomenological model to describe the ferroelectric (FE) and AFE phase transitions based on the Ginzburg-Landau-Devonshire theory. It was applied to the Sm-doped BFO system to study the FE and AFE phase transitions under the Sm doping and pressure. The calculated temperature-composition and temperature-pressure phase diagrams show that the compressive hydrostatic pressure and Sm doping have similar effects on the FE and AFE phase transitions. The results also demonstrate that the intermediate phase of pure BFO under pressure between 3 GPa and 10 GPa is the PbZrO₃-like AFE phase, and that the sequence of phase transitions is from FE to AFE to paraelectric with increasing pressure. Although the current study is under hydrostatic pressure, the model can be easily modified to study the AFE and FE phase transitions under uniaxial and biaxial stresses. The proposed model is general and applicable to other AFE systems.

This work was supported by the NSF MRSEC under Grant No. DMR-0820404, DMR-1410714, and DMR-1210588 (Xue and Gu), the U.S. Department of Energy, Office of Basic Energy Sciences, Division of Materials Sciences and Engineering under Award No. FG02-07ER46417 (Chen).

¹F. Jona and G. Shirane, *Ferroelectric Crystals* (The MacMillan Company, New York, 1962).

²D. Berlincio, *IEEE Trans. Sonics Ultrason.* **SU13**, 116 (1966); W. Y. Pan, C. Q. Dam, Q. M. Zhang, and L. E. Cross, *J. Appl. Phys.* **66**, 6014 (1989).

³J. P. Dougherty, U.S. patent 5,545,184 (13 August 1996).

⁴C. Kittel, *Phys. Rev.* **82**, 729 (1951).

⁵G. Shirane, E. Sawaguchi, and Y. Takagi, *Phys. Rev.* **84**, 476 (1951).

⁶L. E. Cross, *J. Phys. Soc. Jpn.* **23**, 77 (1967); K. Okada, *J. Phys. Soc. Jpn.* **27**, 420 (1969).

⁷M. J. Haun, T. J. Harvin, M. T. Lanagan, Z. Q. Zhuang, S. J. Jang, and L. E. Cross, *J. Appl. Phys.* **65**, 3173 (1989).

⁸E. V. Balashova and A. K. Tagantsev, *Phys. Rev. B* **48**, 9979 (1993).

⁹A. K. Tagantsev, K. Vaideeswaran, S. B. Vakhrushev, A. V. Filimonov, R. G. Burkovsky, A. Shaganov, D. Andronikova, A. I. Rudskoy, A. Q. R. Baron, H. Uchiyama, D. Chernyshov, A. Bosak, Z. Ujma, K. Roleder, A. Majchrowski, J.-H. Ko, and N. Setter, *Nat. Commun.* **4**, 2229 (2013); J. Hlinka, T. Ostapchuk, E. Buixaderas, C. Kadlec, P. Kuzel, I. Gregora, J. Kroupa, M. Savinov, A. Klic, and J. Drahokoupil, *Phys. Rev. Lett.* **112**, 197601 (2014).

¹⁰D. Berlincourt, B. Jaffe, and H. H. A. Krueger, *J. Phys. Chem. Solids* **25**, 659 (1964).

¹¹M. Avdeev, J. D. Jorgensen, S. Short, G. A. Samara, E. L. Venturini, P. Yang, and B. Morosin, *Phys. Rev. B* **73**, 064105 (2006).

¹²P. Yang and D. A. Payne, *J. Appl. Phys.* **80**, 4001 (1996).

¹³I. J. Fritz and J. D. Keck, *J. Phys. Chem. Solids* **39**, 1163 (1978).

¹⁴G. Catalan and J. F. Scott, *Adv. Mater.* **21**, 2463 (2009).

¹⁵D. C. Arnold, K. S. Knight, F. D. Morrison, and P. Lightfoot, *Phys. Rev. Lett.* **102**, 027602 (2009); R. Palai, R. S. Katiyar, H. Schmid, P. Tissot, S. J. Clark, J. Robertson, S. A. T. Redfern, G. Catalan, and J. F. Scott, *Phys. Rev. B* **77**, 014110 (2008).

¹⁶C. J. Cheng, D. Kan, S. H. Lim, W. R. McKenzie, P. R. Munroe, L. G. Salamanca-Riba, R. L. Withers, I. Takeuchi, and V. Nagarajan, *Phys. Rev. B* **80**, 014109 (2009).

- ¹⁷C. J. Cheng, A. Y. Borisevich, D. Kan, I. Takeuchi, and V. Nagarajan, *Chem. Mater.* **22**, 2588 (2010).
- ¹⁸M. Kubota, K. Oka, Y. Nakamura, H. Yabuta, K. Miura, Y. Shimakawa, and M. Azuma, *Jpn. J. Appl. Phys., Part 1* **50**, 09ne08 (2011).
- ¹⁹D. Kan, L. Palova, V. Anbusathaiah, C. J. Cheng, S. Fujino, V. Nagarajan, K. M. Rabe, and I. Takeuchi, *Adv. Funct. Mater.* **20**, 1108 (2010).
- ²⁰S. Karimi, I. M. Reaney, Y. Han, J. Pokorny, and I. Sterianou, *J. Mater. Sci.* **44**, 5102 (2009).
- ²¹K. M. Rabe, *Functional Metal Oxides: New Science and Novel Applications* (Wiley-VCH, 2013), p. 221.
- ²²D. Vanderbilt and M. H. Cohen, *Phys. Rev. B* **63**, 094108 (2001).
- ²³V. V. Lemanov, *Phys. Solid State* **39**, 1468 (1997).
- ²⁴M. Guennou, P. Bouvier, G. S. Chen, B. Dkhil, R. Haumont, G. Garbarino, and J. Kreisel, *Phys. Rev. B* **84**, 174107 (2011).
- ²⁵H. W. Jang, S. H. Baek, D. Ortiz, C. M. Folkman, R. R. Das, Y. H. Chu, P. Shafer, J. X. Zhang, S. Choudhury, V. Vaithyanathan, Y. B. Chen, D. A. Felker, M. D. Biegalski, M. S. Rzchowski, X. Q. Pan, D. G. Schlom, L. Q. Chen, R. Ramesh, and C. B. Eom, *Phys. Rev. Lett.* **101**, 107602 (2008).
- ²⁶V. E. Yurkevich, B. N. Rolov, and H. E. Stanley, *Ferroelectrics* **16**, 61 (1977).
- ²⁷D. Lebeugle, D. Colson, A. Forget, M. Viret, P. Bonville, J. F. Marucco, and S. Fusil, *Phys. Rev. B* **76**, 024116 (2007).
- ²⁸F. Kubel and H. Schmid, *Acta Crystallogr., Sect. B: Struct. Sci.* **46**, 698 (1990); J. X. Zhang, Y. L. Li, Y. Wang, Z. K. Liu, L. Q. Chen, Y. H. Chu, F. Zavaliche, and R. Ramesh, *J. Appl. Phys.* **101**, 114105 (2007).
- ²⁹R. Haumont, P. Bouvier, A. Pashkin, K. Rabia, S. Frank, B. Dkhil, W. A. Crichton, C. A. Kuntscher, and J. Kreisel, *Phys. Rev. B* **79**, 184110 (2009).
- ³⁰D. P. Kozlenko, A. A. Belik, A. V. Belushkin, E. V. Lukin, W. G. Marshall, B. N. Savenko, and E. Takayama-Muromachi, *Phys. Rev. B* **84**, 094108 (2011).
- ³¹W. S. Slaughter, *The Linearized Theory of Elasticity* (Birkhäuser Boston, 2001).
- ³²A. F. Devonshire, *Adv. Phys.* **3**, 85 (1954).
- ³³C. P. Bean and D. S. Rodbell, *Phys. Rev.* **126**, 104 (1962).
- ³⁴B. Jaffe, W. R. J. Cook, and H. Jaffe, *Piezoelectric Ceramics* (Academic Press, London, 1971).
- ³⁵Z. G. Wu and R. E. Cohen, *Phys. Rev. Lett.* **95**, 037601 (2005).
- ³⁶R. Haumont, J. Kreisel, and P. Bouvier, *Phase Transitions* **79**, 1043 (2006).
- ³⁷A. A. Belik, H. Yusa, N. Hirao, Y. Ohishi, and E. Takayama-Muromachi, *Chem. Mater.* **21**, 3400 (2009).
- ³⁸G. A. Samara, *Phys. Rev. B* **1**, 3777 (1970).